

We are IntechOpen, the world's leading publisher of Open Access books Built by scientists, for scientists

6,900

Open access books available

186,000

International authors and editors

200M

Downloads

Our authors are among the

154

Countries delivered to

TOP 1%

most cited scientists

12.2%

Contributors from top 500 universities



WEB OF SCIENCE™

Selection of our books indexed in the Book Citation Index
in Web of Science™ Core Collection (BKCI)

Interested in publishing with us?
Contact book.department@intechopen.com

Numbers displayed above are based on latest data collected.
For more information visit www.intechopen.com



Advanced Optical Imaging of Endocytosis

Jesse S. Aaron and Jerilyn A. Timlin

Additional information is available at the end of the chapter

<http://dx.doi.org/10.5772/45890>

1. Introduction

Endocytosis is the highly controlled and complex process by which a portion of the plasma membrane, including its lipids, proteins, and local extracellular fluid becomes internalized in a cell. Endocytosis serves to mediate a multitude of interactions between a cell and its environment, including nutrient uptake, mitosis, motility, as well as adaptive and innate immune response, among many others. There are multiple routes of endocytotic uptake into cells, with the most studied being clathrin mediated endocytosis (CME). Although CME differs significantly on a molecular level from the clathrin-independent endocytosis mechanisms (e.g. macropinocytosis, phagocytosis), all of the endocytic mechanisms involve a sequence of changes in morphology, molecular composition, and protein interactions at the plasma membrane, as well as throughout the bulk of the cell. Further, each of these changes is tightly regulated in space and time. To fully characterize endocytic pathways and their intertwined relationship to other signalling pathways, there is a need to visualize the dynamics of multiple species at the plasma membrane and within the cell with high three-dimensional spatial resolution.

Traditional biochemical and genetic approaches have provided, and will continue to provide, a wealth of information about the cellular pathways and key molecules involved in endocytosis. However, such bulk assays are only able to provide ensemble measurements. Thus, they cannot shed light on the important and stochastic sub-cellular spatiotemporal information that is inherent to endocytosis. High resolution electron microscopy studies can address this limitation with exquisite spatial detail approaching atomic resolution, but cannot easily capture the dynamics of endocytosis. For this reason, live cell fluorescence microscopy has been exploited to provide vital information at the subcellular and single molecule level about the localization of components involved in individual endocytosis events.

Very early optical microscopy investigations used traditional organic fluorophores and widefield fluorescence imaging to follow membrane associations during endocytosis.

Widefield fluorescence microscopy is readily available, simple to conduct, and provides lateral spatial resolution of 200–400 nm when using visible excitation light and axial spatial resolution on the order of 1 μm with optimal objective and microscope configurations. This resolution is sufficient to understand the overall arrangement of proteins on the cellular membrane and determine uptake into cells as demonstrated by Leserman et al. (Leserman, et al., 1980); but, the presence of interfering signal from throughout the depth of the cell limits the ability to visualize single events using this approach. The addition of the confocal pinhole into the fluorescence microscope serves to reject much of the out-of-focus light, providing a significant improvement in axial spatial resolution, and signal to noise (SNR); confocal fluorescence microscopy has demonstrated wide success in following endocytotic processes within living cells in three dimensions (Betz, et al., 1996; Muller, 2006). The reader is referred to Stephens and Allan for a review of the basics of widefield and confocal fluorescence microscopy technologies for live cell imaging (Stephens & Allan, 2003).

In this chapter, we will summarize optical imaging methodologies beyond the simple transmission optical, widefield fluorescence, and confocal fluorescence microscopes. The advanced techniques presented here have significant advantages in spatial, spectral, and/or temporal resolution when compared to traditional microscopy methods and are well-suited for real-time tracking of individual endocytotic events in living cells. We will cover: (1) total internal reflection fluorescence microscopy, which has become a dominant technology for endocytosis dynamics due to its specificity for the plasma membrane, (2) super-resolution microscopy, whose exquisite spatial resolution has led to emerging applications in the field of endocytosis, and (3) spectral imaging, which exploits the spectral properties of fluorophores and spectral deconvolution to extend fluorescence microscopy much further into the multiplexed regime. In each of these areas, we will introduce the basic concepts of the measurement technique, present important developments in analysis algorithms, and highlight recent studies with regard to endocytosis. It is important to note that although the focus of this chapter is advanced optical imaging methodologies for following endocytosis in living cells, the techniques presented here demonstrate the potential utility in visualizing exocytotic processes and the various vesicle trafficking events that are critical to cell function.

2. Total internal reflection fluorescence microscopy

2.1. Basic principles

Total internal reflectance fluorescence (TIRF) microscopy offers a unique approach for selective imaging of biological components and events very near (typically <200nm) to the plasma membrane in cells (Axelrod, 2001). This technique avoids much of the background signal emanating from fluorophores within the cytoplasm, thereby increasing detection sensitivity over traditional widefield or confocal microscopy. TIRF was first demonstrated in living cells by Axelrod and colleagues for visualization of acetyl choline receptors, and as a sensitive measure of membrane topology (Axelrod, 1981). It has since been widely adopted in biological laboratories for a large range of applications, particularly after the introduction

of commercially available objective-based TIRF systems (Mattheyses & Axelrod, 2006). Demonstrations have included characterizations of cell receptor distributions (N. L. Thompson, et al., 1997), and other membrane bound biomolecules (Sund & Axelrod, 2000), dynamic imaging of exocytic/secretory vesicle trafficking and fusion (Schmoranzler, et al., 2000), as well as single molecule (Tokunaga, et al., 1997) and single nanoparticle (Aaron, et al., 2011) 2D tracking within the membrane. In addition, TIRF has allowed for enhanced biophysical characterizations of endocytotic events, as discussed in the following section.

The principle behind TIRF relies on the creation of evanescent excitation. Snell's law accurately predicts the angle of light refraction through media of various refractive indices. However, it can be shown that in cases where light propagates from a higher refractive index material (such as glass) to a lower refractive index material (such as air or water), there exists a critical angle, θ_c , above which refraction cannot occur. Mathematically, this is represented by:

$$\theta_c = \sin^{-1}\left(\frac{n_1}{n_2}\right) \quad (1)$$

where n_1 and n_2 correspond to the lower and higher refractive indices, respectively. At angles that exceed this value, total internal reflection occurs, and light does not propagate through the lower refractive index material, but rather is reflected away from the interface in the opposite direction. Interestingly, a more detailed analysis using Maxwell's equations reveals that a portion of the impinging light's energy extends slightly into the lower refractive index material. This is referred to as an evanescent wave, which propagates parallel to the interface, and decays quickly in the perpendicular direction. The decrease in intensity from the surface can be described by an exponential function, with characteristic decay constant, d , given by:

$$d = \frac{\lambda}{4\pi} \left(n_2^2 \sin^2 \theta - n_1^2 \right)^{-\frac{1}{2}} \quad (2)$$

where λ refers to the excitation wavelength, θ is the angle at which the light impinges normal to the interface ($\theta > \theta_c$), and n_1 and n_2 are as described above. Equation (2) indicates that the penetration depth of the evanescent field will typically extend a distance less than the wavelength of light used, and will decrease with increasing illumination angle. For instance, excitation at 532nm, passing from a glass coverslip ($n_1 = 1.52$) to an aqueous environment ($n_2 = 1.33$), at an angle of 68° to the surface, will exhibit an evanescent decay length of only 165nm. This represents more than a 3-fold smaller distance than the axial resolution of a typical confocal microscope. As such, TIRF has become a widely used modality to study events very near the cell membrane, including the myriad of endocytosis mechanisms. The following sections focus on three phenomena where TIRF imaging has dramatically impacted current knowledge of internalization-related phenomena: (1) clathrin mediated endocytosis, (2) cellular uptake of viruses, and (3) internalization of engineered nanoparticles.

2.2. Understanding clathrin mediated endocytosis via TIRF microscopy

CME is perhaps the best characterized pathway for internalizing receptor-specific biomolecules and is conserved among nearly all eukaryotic cells (Rappoport, et al., 2004). Many of the earliest studies examining CME relied on electron microscopy due to the ultra-high resolving power of that modality (Kirchhausen, et al., 1986). However, the advent of fluorescence imaging has permitted the important advantage of capturing dynamic, molecular-specific behavior in living cells. When combined with fluorescent protein constructs or other labels, new insights into this complex process have been gleaned using time-resolved live cell microscopy.

Earlier wide-field fluorescence imaging studies reported previously unseen behavior of clathrin-coated pits (CCPs) on or near the plasma membrane (Gaidarov, et al., 1999). Interestingly, distinct patterns were observed within a cell-wide population of CCPs. A majority of CCPs displayed limited/random, or no lateral motion within the membrane, and were generally termed “static”. With the introduction of TIRF microscopy, a subset of CCPs was observed to be motile – exhibiting rapid active transport motion (Keyel, et al., 2004). This latter observation has led to a shift in the overall model of the CME pathway. While clathrin was originally thought to only participate in vesicle formation, Rappoport et al. showed that some clathrin coated vesicles (CCVs) persisted beyond the initial plasma membrane-bound state, and were transferred to microtubules parallel to the membrane (Rappoport, Taha, & Simon, 2003). This rapid motion was correlated with CCV internalization. However, still others were shown to disappear or re-appear from the TIRF field of view without active transport-like motion. This suggested that some disassembly or reassembly of the clathrin triskelia is concomitant with their internalization away from the evanescent field, without transport by motor proteins/microtubule network (Merrifield, et al., 2002; Merrifield, et al., 2005).

Matters were complicated further when later data suggested that a single CCP could give rise to multiple vesicles (Rappoport, 2008). Single particle analysis of TIRF data showed that some CCV were initiated *de novo* – that is, the assembly of a single CCP resulted in complete disappearance of clathrin-associated signal into an internalized vesicle. However, other CCPs were seen to separate into sub-structures, only a portion of which were seen to internalize, while other CCPs were seen to merge into larger structures (often termed clathrin coated plaques). As an example, Figure 1 shows TIRF images and analysis representing a single event of the latter type, taken from (Rappoport, 2008). Close inspection of the indicated point spread function from a single sub-diffraction sized CCP shows a broadening and eventual separation into two distinct features. This was followed by the disappearance of the newly isolated CCP, presumably as it is internalized as a vesicle. This model of CCV formation has been referred to as iterative budding. The relative contributions of *de novo* formation and iterative budding mechanisms to overall CME behavior have shown to be highly cell-line dependent. Swiss 3T3 fibroblasts exhibited 59%:41% iterative:*de novo* behavior in one study (Merrifield, et al., 2005), while BSC1 cells showed exclusively *de novo* CCV formation in another (Ehrlich, et al., 2004).

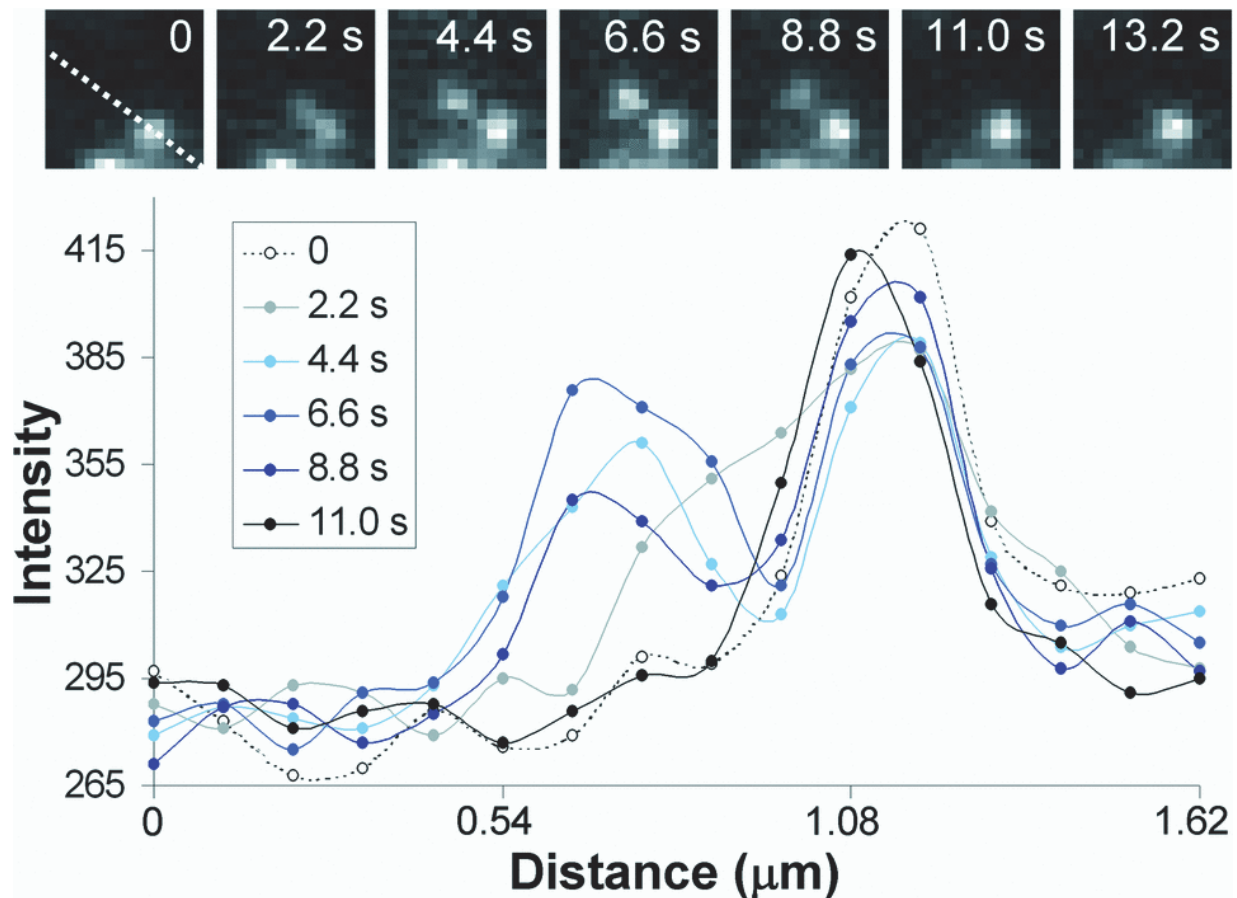


Figure 1. Iterative budding of a CCV from a larger CCP. At top, an image sequence illustrates TIRF images of CME. At bottom, signal intensity profiles indicate the progressive widening of a single CCP, and eventual partial separation, resulting in the iterative budding of a single CCV (Rappoport, 2008). Reproduced with permission, from Rappoport, (2008), *Biochem. J.*, **412**, 415-523. © The Biochemical Society.

The complexity and mechanistic diversity of CME has been postulated to arise in part from variety of adapter and accessory proteins that are expressed in a given cell. However, there does appear to be a “core” group of molecular players present in nearly all forms of CME. Arguably the most ubiquitous accessory proteins are dynamin and actin. Dynamin fulfills a plethora of roles within many cell signaling pathways (particularly dynamin-2). One of its most prominent functions is in aiding the initial formation of CCVs, and their scission from the plasma membrane. Despite its importance, the precise sequence of events surrounding the role of dynamin is still uncertain. Merrifield et al. initially showed, via dual-color TIRF microscopy, an increase in dynamin-associated fluorescence immediately prior to clathrin internalization, and a synchronized decrease during CCV internalization (Merrifield et al., 2002). However, the underlying reason for the increase in fluorescence is still not clear. Alternate models predict either a recruitment of dynamin from the cytosol directly to the “neck” of the newly formed CCV, or recruitment from the cytosol to the whole vesicle, and then translocation to the point of invagination.

Along with dynamin, actin also plays a role in CCV formation as an accessory protein in many cells (Kaksonen, et al., 2006; Merrifield, et al., 2002). Merrifield et al. showed that EGFP-actin signal displayed a transient increase near CCPs during internalization

(Merrifield, et al., 2002). Interestingly, using TIRF microscopy to compare the kinetics of dynamin and actin recruitment over a number of cells clearly indicated that dynamin recruitment consistently precedes local actin polymerization (in addition to clathrin internalization), thus giving valuable insight to the sequence of events in the CME process.

TIRF microscopy has also been instrumental in disentangling the complex interactions of adapter proteins involved in CME (Rappoport, et al., 2006). The first identified, and most studied, of these are the adaptins (Boehm & Bonifacino, 2001). These proteins can form a tetrameric complex referred to as AP-2, and act as an intermediate between cell surface receptors and the endocytic machinery by concentrating cargo bound for internalization into a CCP. However, the role for AP-2 during the post-internalization phase has been controversial. Rappoport et al. initially showed that AP-2 is lost from the CCV during internalization (Rappoport, Taha, Lemeer, et al., 2003), although Keyel et al. later proposed that AP-2 accompanies CCVs into the cytosol, suggesting its possible regulatory role the downstream sorting machinery (Keyel, et al., 2004). However, more detailed TIRF image analysis confirmed the former hypothesis, and showed that while AP-2 was co-localized to static CCPs in the membrane, it was absent from those CCPs observed to disappear into the cytosol (Rappoport, et al., 2005).

2.3. Tracking single viruses and endocytosis in living cells with TIRF imaging

Similar to its utility in understanding the kinetics of endogenous protein-protein interactions during CME, TIRF microscopy has also been highly useful to probe the mechanisms of pathogen invasion via similar routes. Of particular interest is the mechanism by which viruses enter their host cells (Brandenburg & Zhuang, 2007). Although some viruses (such as HIV) replicate via direct genome injection through the plasma membrane, most have evolved a multitude of methods to gain entry to cells via endocytosis; specific mechanisms include CME, macropinocytosis, and caveolin-dependent internalization (Sieczkarski & Whittaker, 2002a). As a prominent example, this section will highlight studies of Influenza A viral entry by CME, as elucidated by TIRF microscopy.

Zhuang and colleagues were among the first to visualize the interactions between single influenza A viruses and host cells using both widefield (Lakadamyali, et al., 2003) and TIRF microscopy (Floyd, et al., 2008; Rust, et al., 2004). Influenza A is an enveloped, single-stranded RNA virus thought to enter cells via CME, although more recent data indicate it may also utilize a clathrin-independent pathway (Sieczkarski & Whittaker, 2002b). One of the first TIRF imaging studies revealed that influenza A particles were internalized via *de novo* CCP formation and internalization to CCV, as shown in Figure 2 (Rust, et al., 2004).

Images indicate that Influenza viruses, which were labeled with a lipophilic fluorescent tracer (DiD, shown in red), bind to the surface of live BSC1 cells. A few minutes after binding, GFP-tagged clathrin is seen to accumulate around a subset of viral particles, as shown in (B). Following this, the velocity of the viral particle dramatically increases, indicative of attachment to microtubules. The increase in viral velocity is then correlated with a complete disappearance of both DiD and GFP fluorescence signal, suggesting

directed internalization within a single, *de novo* CCV. Interestingly, however, some viral particles were seen to exhibit the aforementioned velocity increase without apparent recruitment of clathrin. While that may simply suggest the presence of non-fluorescent clathrin, it may also point to the presence of alternate endocytosis mechanisms. This later hypothesis is supported by other data that demonstrate little change in influenza infectivity in the presence of inhibitors of CME (Sieczkarski & Whittaker, 2002b). Nevertheless, CME does seem to be a route that is well-exploited by viral pathogens, albeit not always in the classical sense. For instance, Johannsdottir, et al. used single particle tracking TIRF microscopy to show that while dynamin-2 was required for Vesicular stomatis virus (VSV) internalization, AP-2 was not (Johannsdottir, et al., 2009).

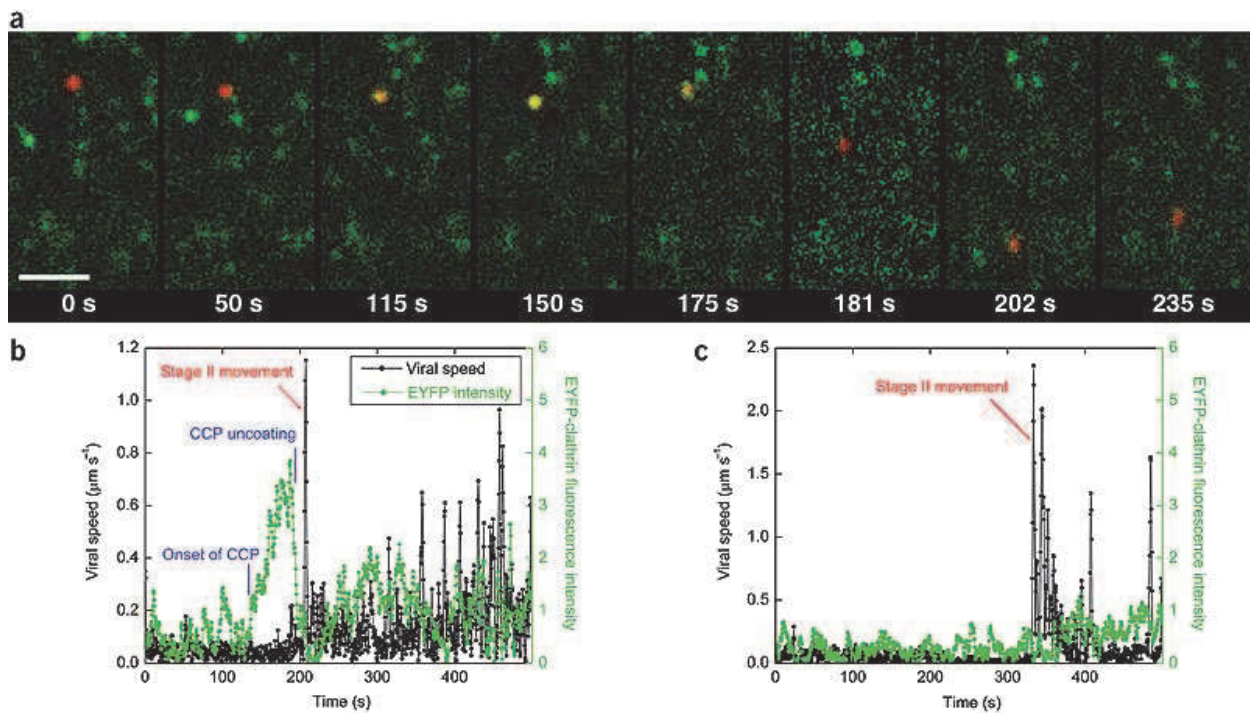


Figure 2. Dual color TIRF microscopy reveals that Influenza virus is endocytosed via *de novo* CCV formation. In (a), a single influenza virus (shown in red) binds to the cell surface, and is eventually colocalized to EGFP-tagged clathrin. After colocalization, the clathrin/virus complex displays enhanced motility, and eventual disappearance from the evanescent field. In (b), intensity profiles (in green) show the recruitment of clathrin near the single influenza virus. Black traces indicate viral velocity, indicative of active transport into the cytoplasm. In (c), an example of viral internalization is shown that does not indicate dependence on clathrin (Rust, et al., 2004). Adapted by permission from Macmillan Publishers Ltd: Nature Structural and Molecular Biology M.J. Rust, et al., **11**(5), 567-573, © 2004.

TIRF microscopy has been used to not only visualize initial viral entry, but also its behavior later in the endocytosis pathway. When enveloped viruses are labeled with high density of a fluorescent dye such as DiD or lipophilic Rhodamine, fluorescence self-quenching occurs such that viral particles are relatively non-fluorescent. Upon fusion of the virus to the endosomal membrane, the density of fluorophore decreases, resulting in a dramatic increase in detectable signal (Hoekstra, et al., 1984; van der Schaar, et al., 2007). Furthermore, viral particles can independently or simultaneously be loaded with a tracer molecule to measure

release of genomic material into the cytosol, subsequent to fusion (Brandenburg, et al., 2007). For instance, Floyd, et al. used a dual-labeling approach to gain new insights into influenza fusion using a supported lipid bilayer model under TIRF interrogation as shown in Figure 3 (Floyd, et al., 2008).

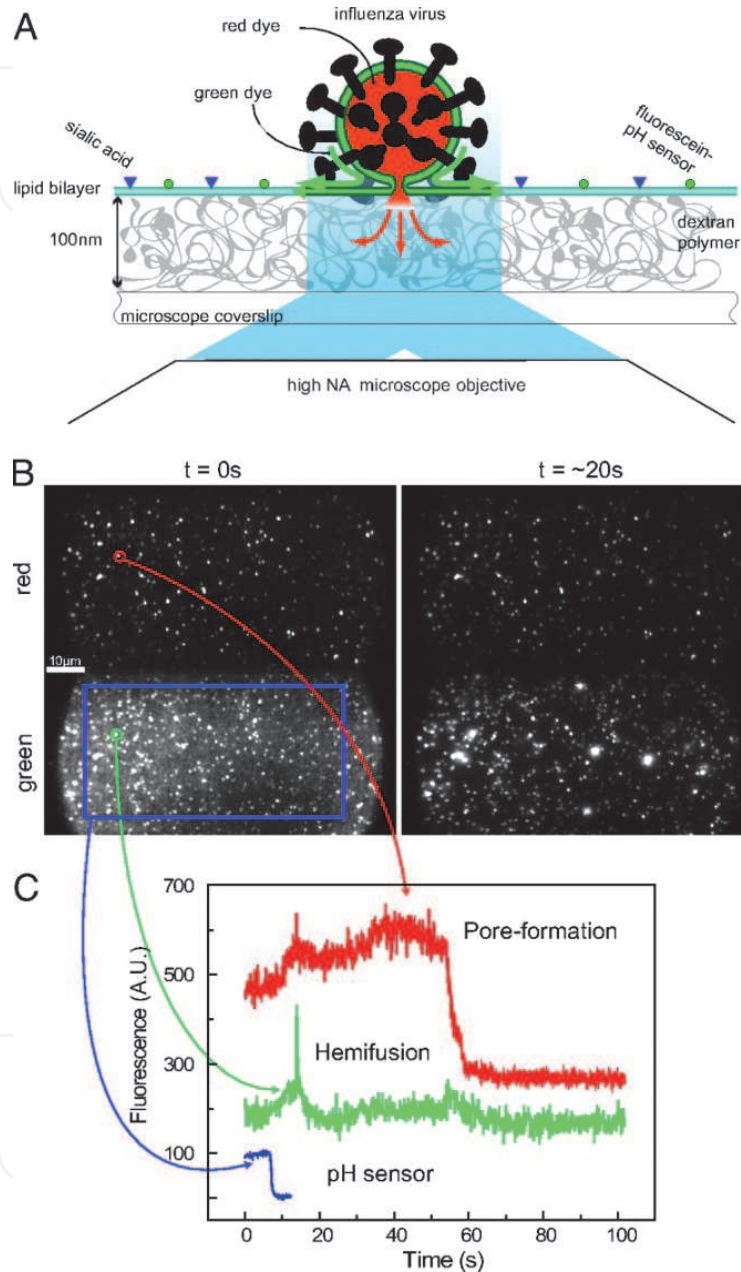


Figure 3. In vitro TIRF characterization of influenza fusion and content mixing. In (A), the experimental setup is illustrated, showing influenza virus binding to a dextran-supported lipid bilayer to model the endosomal membrane. Viral envelopes are labeled with lipophilic rhodamine (green), and the interior is loaded with sulforhodamine B (SRB) (red). Images in (B) show representative dual color TIRF images. In (C), fluorescence intensity plots show a sharp spike in the lipophilic rhodamine signal (green), indicative of viral hemifusion, while the SRB (red) shows the dispersal of viral cargo into the sub-bilayer space after pore formation (Floyd, et al., 2008). *Reproduced with permission, from D.L. Floyd, et al., Proc. Nat. Acad. Sci., 105(40), 15382-15387, ©2008 by the National Academy of Sciences.*

In this study, influenza viruses were labeled first with a lipophilic Rhodamine derivative, which exhibits a fusion dependent signal increase under these conditions. Additionally, the interior of the virus was labeled with sulforhodamine B (SRB). While only 30% of virus contained both dyes in sufficient quantities, the sequence of viral docking, fusion, and content release was able to be monitored in near real time, and corresponding rate constants, number of intermediate states, and lag times between fusion and pore formation were all able to be calculated. Figure 3 shows TIRF experimental setup (A) and data (B-C) obtained from influenza virus interactions with a liquid supported bilayer. In (C), dual color TIRF microscopy shows pore formation (red) vs. hemifusion (green) as a function of time. Hemifusion can be detected by a sharp, transient increase in fluorescence intensity as the lipophilic dye is released from its self-quenching state, and diffuses throughout the bilayer. The viral content release is assessed by the decay in red fluorescence as the SRB enters the sub-bilayer space and diffuses away.

As can be seen, TIRF microscopy has produced notable insight into pathogenic infection mechanisms, particularly with regard to their endocytosis by host cells. As opposed to bulk studies, imaging approaches allow for a “single cell”, and even “single virus” quantification of behavior. This capability has far-reaching consequences in understanding fundamental molecular mechanisms. For instance, the data above was used to model the kinetics of viral hemifusion with endosomal membranes to clearly reveal that three intermediate stages exist in this process, thereby opening avenues for potential, specific therapeutic targets for Influenza infection.

2.4. TIRF microscopy for studying endocytosis of engineered nanomaterials

In addition to monitoring the internalization of pathogens, TIRF microscopy has also been instrumental in characterizing the uptake of engineered nanoparticles aimed at therapeutic or diagnostic applications (West & Halas, 2003), as well as in an effort to assess possible toxicological consequences of these materials (Marquis, et al., 2009). Engineered nanoparticles comprised of porous silica (Slowing, et al., 2008), liposomes (Hashida, et al., 2005), and other polymer materials (Panyam & Labhasetwar, 2003) have been widely successful as therapeutic carriers for both drug and gene delivery. Much of these approaches depend on the endocytic uptake and release of the material in question into the cytoplasm. Thus, quantitative characterizations of endocytosis are imperative in order to assess diagnostic/therapeutic effect.

Among the first and most widely used nanomaterials for diagnostic use include quantum dots (QDs). QDs are typically <20nm in diameter, and are comprised of various heavy metal/semiconductor materials such as CdSe, CdTe, or PbS, among others. This configuration results in an electronic bandgap that typically falls in the optical/NIR wavelength range. As such, QDs make highly attractive optical imaging probes with narrow emission bandwidth, broad absorption spectra, and relative resistance to photobleaching (Medintz, et al., 2005). Nie and colleagues were the first to demonstrate their utility as molecular imaging probes (Chan & Nie, 1998), and they have since gained wide-spread acceptance in this regard, including their use as *in vivo* diagnostic agents (Gao, et al., 2005).

Nevertheless, questions remain about the possible cytotoxic effects of semiconductor/heavy metal nanomaterials. In this regard, TIRF microscopy has been utilized to quantify the uptake properties of various CdSe QDs in immune cells. Aaron et al. have shown that while QD diameter is not a good predictor of cellular uptake (both in terms of uptake rate and extent), there does appear to be a correlation with QD shape (Aaron, et al., 2011). Figure 4 shows representative TIRF images of QD (emitting at 605nm, referred to as QD605) uptake in RBL mast cells over time. Similar to studies examining CME, this approach relied on the gradual disappearance of QD-associated signal as particles are transported to the cytoplasm, and away from the evanescent field.

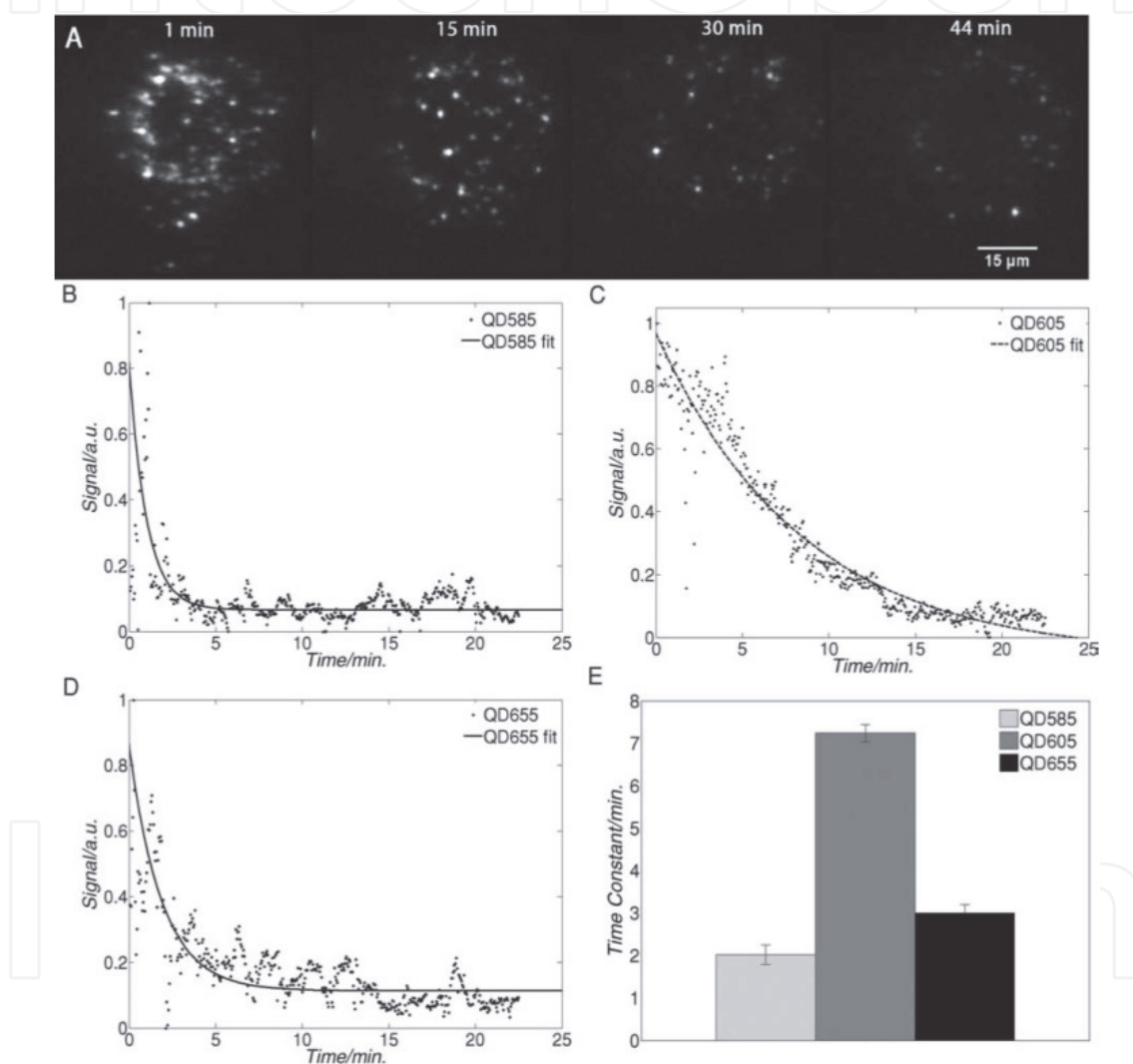


Figure 4. TIRF microscopy to quantify internalization rates of various shape/size quantum dots (QDs) in an RBL mast cell line. In (A), fluorescence signal from QDs are seen to gradually disappear over 30-60 minutes, as they move beyond the TIRF evanescent field into the cytoplasm. The total QD signal can be plotted vs. time to calculate a characteristic endocytosis time (B-D) for various sized/shaped QDs. These values are represented in (E) for two spheroidal QDs (QD585 and QD655, in light and dark grey, respectively), and one rod-shaped QD (QD605, medium grey). Data suggest that particle shape regulates internalization, with uptake times of rod-shaped particles nearly two-fold longer than spheroidal QDs (Aaron, et al., 2011).

Live cell time-course TIRF imaging of QD uptake (shown in A) allows for a measure of endocytosis rates for these materials. By simply plotting fluorescence signal as a function of time, a typical decay behavior becomes evident. Uptake measurements taken for QDs emitting at 585nm, 605nm, and 655nm (B, C, and D, respectively) showed marked differences in their rates of internalization, summarized in (E). Interestingly, the uptake rates did not correlated with size (average diameter increases with increasing emission peak), but upon closer inspection, was found to be related to QD shape. While QD585 and QD655 displayed relatively small aspect ratios (1.2 and 1.6, respectively), QD605 were found to have more rod-shaped character, with aspect ratio of 2.0. This suggests that spheroidal particles are internalized at a higher rate than elliptical particles, giving insight into the shape and size effects on nanoparticle-cell interactions.

2.5. Emerging TIRF microscopy methods

TIRF microscopy is currently in the midst of another renaissance, as more advanced methodologies are being developed to better extract meaningful, quantitative information about events at the plasma membrane. Two such approaches are directly applicable to imaging of endocytosis, and include polarization sensitive and multi-angle TIRF imaging.

Polarization-sensitive TIRF (pTIRF) microscopy had been proposed for some time (N. L. Thompson, et al., 1984), yet only in the last several years have these concepts been applied in biological samples (Anantharam, et al., 2010; Sund, et al., 1999). This method is based on the observation that, at the surface of a cell, endocytosis events create a localized birefringent environment, as illustrated in Figure 5. As can be seen, during endocytosis (or exocytosis), the deformation of the plasma membrane creates portions of the membrane that are parallel and perpendicular (as illustrated by arrows) to the s- and p-polarizations of the evanescent field, respectively. Therefore, a polarized detection scheme will be sensitive to separate regions within the nascent vesicle, provided that fluorescent dyes (such as DiD) are all oriented similarly with respect to the lipid bilayer. Resulting images may include a “doughnut” appearance at sites of membrane invagination, due to the alternative parallel and perpendicular orientations of the membrane with respect to the evanescent field polarization. While still in its infancy, this method has sensitively detected exocytosis of neuronal vesicles (Anantharam, et al., 2010), as well as fusion of SNARE-bearing vesicles on a supported lipid bilayer (Kiessling, et al., 2010). Further studies combining pTIRF with atomic force microscopy have shed light on fundamental mechanisms of protein-mediated membrane disordering (Oreopoulos & Yip, 2009).

While technically more complex, pTIRF may also be an ideal method for imaging endocytosis pathways that do not have well identified proteomic markers. For instance, a growing body of evidence has shown that Influenza A virus may make use of multiple endocytic pathways for infection of host cells, with at least one route being both clathrin and caveolin-independent. Using pTIRF to image the structural and kinetic properties of this cryptic pathway may lead to ultimately elucidating its origin.

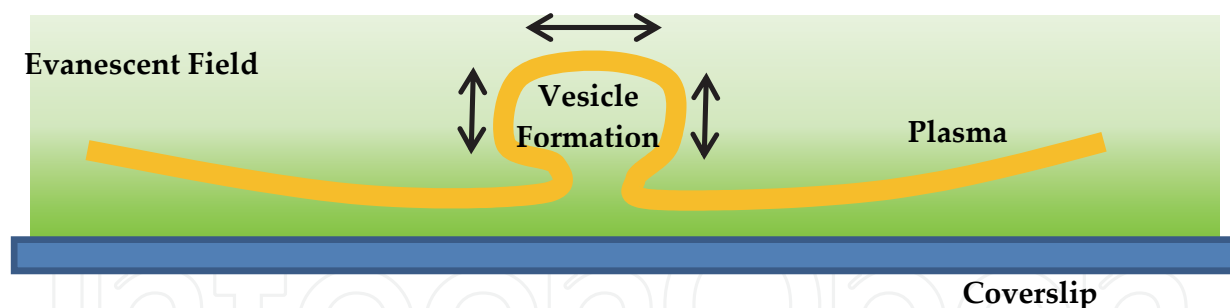


Figure 5. Principle of pTIRF. During membrane reorganization during endocytosis, fluorophores become oriented perpendicular and parallel to the incoming evanescent field polarization. Using cross-polarized detection, endosomal vesicles appear as alternating dark and light rings.

Another promising emerging strategy is the implementation of multi-angle TIRF microscopy. Hypothesized more than 20 years ago (Reichert, et al., 1987), it has only more recently been applied to quantitatively determining axial distributions of biomolecules at the nanoscale. Recall that Equation 2 in section 2.1 illustrates how the evanescent field depth is a sensitive function of illumination angle, with decreasing field penetration with increasing beam angle. This offers the intriguing possibility of optical sectioning at various axial positions near the sample/coverglass interface, far below the optical diffraction limit by systematically varying the TIRF angle, θ . This strategy has been successfully implemented in a compact design (Stock, et al., 2003), and utilized for a number of applications, including mapping cell membrane topology relative to the cytoplasm (Olveczky, et al., 1997), viewing exocytosis of secretory granules in Chromaffin cells (Oheim, et al., 1998), as well as detecting sub-diffraction axial movements of surface-immobilized DNA molecules, all with accuracies of less than 50nm along the optical axis (He, et al., 2005). Doubtless, the application of this methodology may shed new lights into endocytic mechanisms as well.

3. Super-resolution microscopy

3.1. History and background

Until the last decade, interrogation of cells and cellular processes with a microscope was limited by diffraction. Practically speaking, this meant that cellular features could only be distinguished if they were laterally separated by at least half the wavelength of the illumination light, as elegantly described by Ernest Abbe in in the late 19th century (Abbe, 1873). Under visible wavelength excitation, this means that cellular features and structures must be at least 200-350 nm apart in order to be resolved in X and Y. Unfortunately, this resolution limit is more than an order of magnitude larger than the spatial scale on which most biochemical processes occur. To address this, scientists have developed specialty optical microscopy techniques over the years to achieve information on a spatial scale below the limits of optical diffraction in living organisms. The most well-known of these are Förster resonance energy transfer (FRET), fluorescence correlation spectroscopy (FCS), and TIRF microscopy which as discussed above can provide axial resolution of *ca.* 100 nm, but is limited by diffraction in the lateral dimension.

More recent advances have produced several new methodologies, collectively termed “super-resolution” microscopy or “nanoscopy” that effectively break the traditional diffraction barrier in all three spatial dimensions. These resolutions are more aligned with the spatial scales on which biomolecular processes occur, and have potential to re-define the state-of-the art in biological imaging. Though a complete review of all the super-resolution microscopies is outside of the scope of this chapter, this section will discuss two major approaches with demonstrated applications in endocytosis: (1) localization microscopy and (2) stimulated emission depletion microscopy (STED). The reader is referred to recent review articles and the references within for additional information on super-resolution microscopy (B. Huang, et al., 2009; Schermelleh, et al., 2010).

3.2. Localization microscopy

3.2.1. Fundamentals of localization microscopy

If a single molecule within a diffraction-limited volume can be imaged independently from any other nearby emitters, localization techniques (R. E. Thompson, et al., 2002) can be employed to determine that molecule’s location with precision of approximately

$$\Delta x \approx \frac{PSF}{\sqrt{N}} \quad (3)$$

where Δx is the localization precision, PSF is the size of the point spread function, and N is the number of detected photons from a single chromophore. With laser excitation and modern detectors, this accuracy can routinely be accomplished with <50nm precision. Interestingly, if this localization procedure could be repeated for many molecules, then an image could be constructed from the sum of all the localizations, with lateral resolution nearly 10-fold less than the diffraction limit. The practical challenge of this approach is rendering the vast majority of fluorophores in a sample in a “dark” state, only allowing a small subset to be visible at any given time. Indeed, conventional immunofluorescence labelling may result in thousands of visible fluorophores within a diffraction limited volume. However, several methods based on wide-field imaging of subpopulations of molecules activated in a stochastic fashion have emerged, including STORM (Rust, et al., 2006), PALM (Betzig, et al., 2006), and FPALM (Hess, et al., 2006). These approaches, collectively termed localization microscopies, each differ in the photophysics and photochemistry through which the single molecule activation and deactivation is achieved, but in general, make use of some form of “photoswitching” to turn individual fluorescent dyes to/from an on/off state. Then, the localization procedure remains essentially the same as described previously. In each approach, a delicate optimization is necessary between dye choice, imaging buffer solutions, labelling density, excitation wavelength and intensity, emission wavelength, and acquisition speed to produce images of the highest quality. A comprehensive review of fluorophore characteristics for use in localization microscopy has been recently published (Dempsey, et al., 2011).

To visualize biological processes like endocytosis which occur in three-dimensions, it is important to develop techniques that improve spatial resolution in x , y , and z and are compatible with imaging of living cells. More recent methods based on Astigmatism (Huang, Wang, et al., 2008) and dual-focal plane imaging (Juetten, et al., 2008) have achieved axial localization precisions of 50 nm and 75 nm respectively, over depths of several hundreds of nanometers. Additionally, sub- 25 nm axial localization precision has been demonstrated using interferometric methods (Shtengel, et al., 2009). Z-scanning and single-particle tracking can be combined with these methods to extend the depth to several micrometers permitting imaging throughout the cell. (Huang, Jones, et al., 2008; Juetten, et al., 2008). Though localization microscopies were originally limited to imaging fixed cells due to the conditions necessary to provide the stochastic photoswitching and the need to have no movement during the lengthy acquisition times, current methods are compatible with live-cell imaging (Manley, et al., 2008; Shroff, et al., 2008) while still maintaining axial spatial resolutions in the 50-60 nm range. This is an active area of research and further advancements are anticipated to eventually permit visualization of endocytotic dynamics at sub-50 nm resolution in all three dimensions.

3.2.2. Current applications of localization microscopy in endocytosis

The past five years have seen a flurry of localization-based superresolution microscopy studies related to endocytic processes, in a number of contexts. For instance, Betzig et al. successfully detected lysosomal membrane-associated proteins using a PALM approach with better than 10nm lateral resolution in fixed cell sections (Betzig, et al., 2006). Furthermore, Zhuang and colleagues were able to construct exquisite 3D images of both microtubule networks and clathrin coated vesicles (CCVs) in intact samples using the astigmatism-based STORM approach described above (Huang, Wang, et al., 2008). In addition, highly multiplexed studies using another localization variant, ground state depletion followed by individual molecule return (GSDIM), have shed light on the interactions between clathrin, tubulin, actin, and peroxisomes (Testa, et al., 2010). The interactions of HIV with the host cell cofactor tethrin (a protein implicated in preventing virus internalization) were revealed with excellent detail using a combination of photoactivatable proteins and photoswitchable organic dyes (Lehmann, et al., 2011). Another excellent example of super-resolution imaging applied toward endocytosis mechanisms includes a study by Subach, et al. In this case, novel photoactivatable proteins were exploited to acquire dual-color PALM images to visualize the clustering of transferrin receptors into clathrin coated pits (CCPs) at 25nm spatial resolution, as illustrated in Figure 6 (Subach, et al., 2009).

Data in Figure 6 show the substantial increase in image detail afforded by super-resolution imaging (b, e, h) over TIRF microscopy (a, d, g), with enlarged areas (indicated by white boxes), shown in (c, f, i). Clathrin (green) is generally co-localized to clusters of transferrin (red), although a large background of isolated/non-colocalized receptors is also apparent.

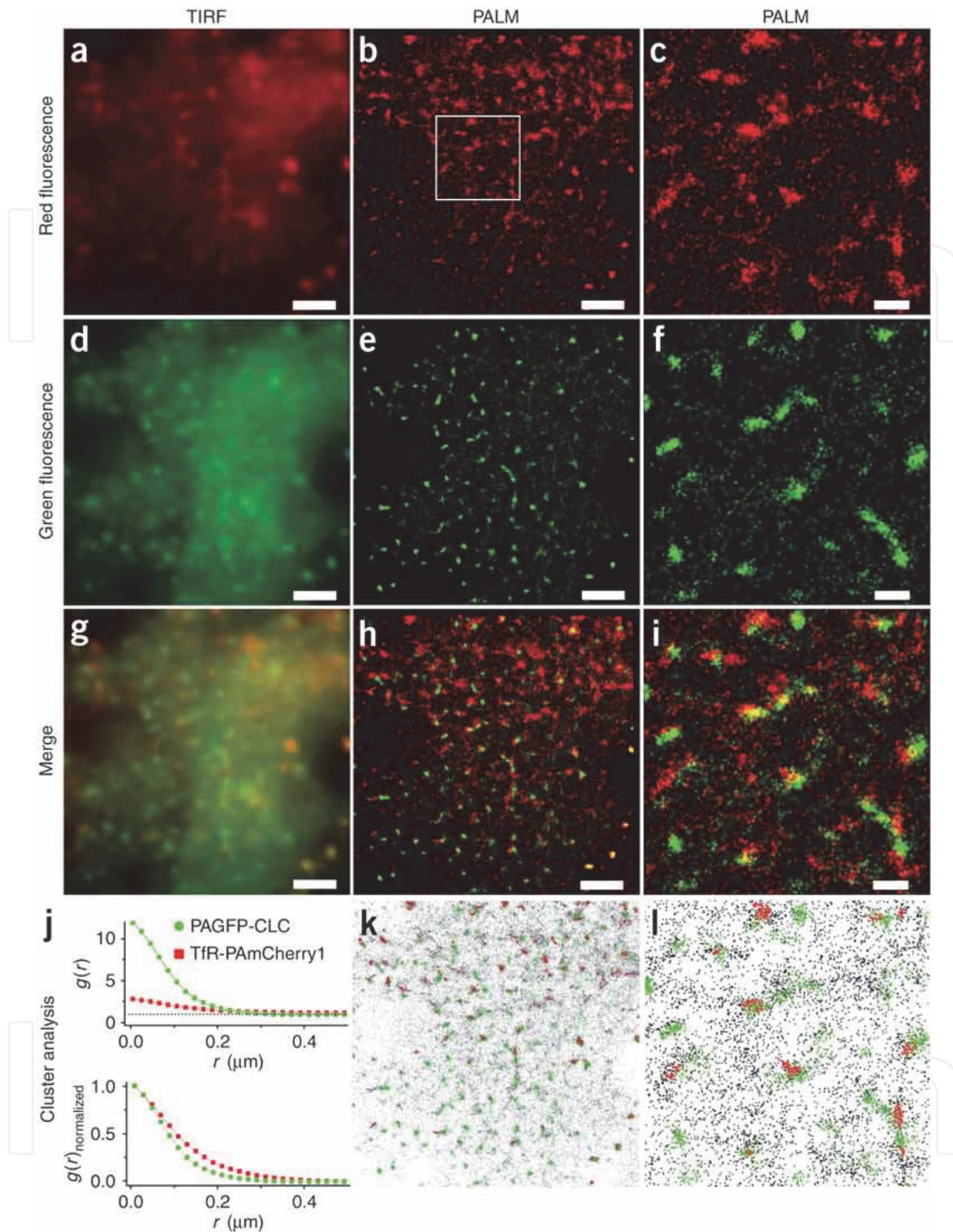


Figure 6. Localization-based super-resolution microscopy of transferrin receptor co-localization to CCPs. (a, d, g) indicate conventional TIRF images of receptor, clathrin, and overlay image, respectively. (b,e,h) illustrate the large increase in image detail after super-resolution localization is performed, with zoomed in regions displayed in (c, f, and i). Co-cluster analysis was performed on areas where transferrin receptor/clathrin density was greater than 5-fold the mean (k, l). Correlation functions indicate a characteristic cluster size of approximately 200nm, below the Abbe limit (j) (Subach, et al., 2009). Reprinted by permission from Macmillan Publishers Ltd: Nature Methods F.V. Subach, et al., 6(2), 153-159, ©2009.

As this data suggests, super-resolution microscopy also allows for image analysis with greatly increased precision over diffraction-limited imaging. In (k-j) receptor/clathrin clusters are analysed such that only areas where receptor density is five-fold greater than the image-wide average are considered (k-i). Spatial pair-correlation analysis (j) gives a measure of cluster diameter in the 200nm range, representing a detailed optical image analysis below the Abbe limit. This is important, as the above treatment demonstrates that while super-resolution imaging can provide images with exquisite detail and multiplexed capability, perhaps its greatest utility is its ability to enable improved quantification of biomolecular behaviour *in situ*. As more demonstrations are reported, new biological insights will doubtless be gained with the ability to monitor changes in biomolecular localization and dynamics at the nanoscale.

3.3. Stimulated emission depletion microscopy

3.3.1. Fundamentals of STED microscopy

In contrast to the localization-based super-resolution methods described in sections 3.1-3.2, stimulated emission-depletion (STED) microscopy relies on a different mechanism, and falls into the category of illumination-based techniques. Instead of localizing many random fields of single fluorophors to form a complete image, illumination-based methods rely on a carefully engineered point spread function (PSF) that effectively limits fluorescence emission to a small, sub-diffraction volume. This modified PSF is subsequently scanned across a field of view in order to construct an image via confocal detection.

By far the most common way to accomplish a restriction in the PSF is to make use of two, superimposed beams of light, as shown in Figure 7. The first “excitation” beam (green) is a conventionally focused laser spot, whose diameter is subject to the diffraction limit. The second “depletion” beam (orange) is also diffraction limited, but a phase function is imparted such that it forms an optical vortex or “doughnut” when focused on the sample. When superimposed, the depletion beam prevents conventional fluorescence emission except for a small area near the center of the vortex. Using this method, optical resolutions approaching 7nm have been achieved (Rittweger, et al., 2009).

The concept of stimulated emission as a means to break the diffraction barrier extends from Stephan Hell’s seminal paper exploring the theoretical basis (Hell & Wichmann, 1994), with experimental demonstration following (Klar, et al., 2000). The original implementation of this concept involved complex, expensive instrumentation, including pairs of highly synchronized, femtosecond pulsed laser sources, in addition to other non-trivial timing electronics. However, subsequent simplifications were made such that STED could be accomplished with a single light source (Wildanger, et al., 2008), as well without any pulsed light sources (Willig, et al., 2007).

STED microscopy remains a very active area of development, with applications demonstrated in a wide variety of fields (Nägerl, et al., 2008; Rittweger, et al., 2009; Willig, Kellner, et al., 2006; Willig, Rizzoli, et al., 2006). Endocytosis stands as an enticing area in which to apply STED microscopy, due to the intricate interplay between proteomic mediators and the sensitive spatiotemporally varying nature of cargo internalization.

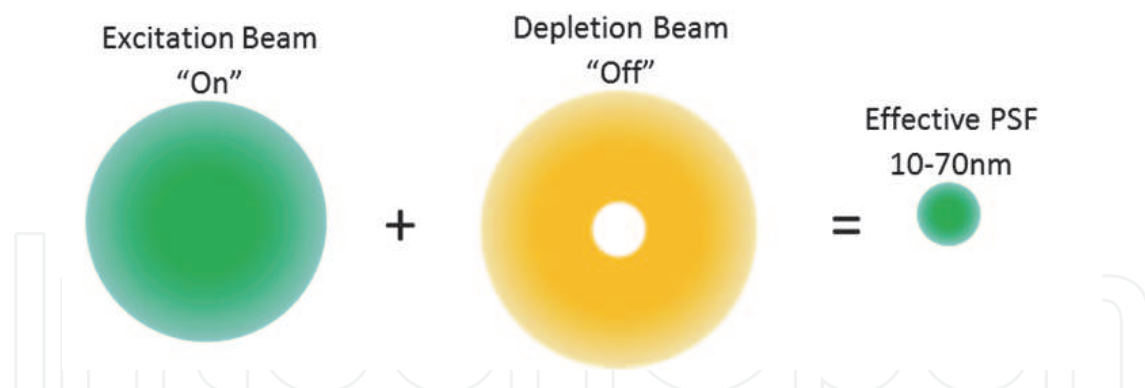


Figure 7. Principle of Stimulated Emission Depletion (STED) Microscopy. A conventional excitation spot (green) is overlaid with an optical vortex depletion beam (orange) to confine fluorescence emission to a sub-diffraction volume, and then scanned across a sample to create an image.

3.3.2. Current applications of STED microscopy in endocytosis

Illumination-based super-resolution techniques such as STED generally require more complex instrumentation as compared to localization approaches such as PALM/STORM. However, STED offers the advantage of more facile dynamic imaging. Although STED-based methods have somewhat lagged in their application toward the understanding of endocytosis as compared to localization techniques, several studies have begun to bring the considerable power of STED microscopy to bear on a number of pathways that are relevant in this regard. For instance, Schneider, et al. utilized STED microscopy to gain insight into the function of flotillin proteins in the context of Alzheimer's disease. Flotillins have been implicated in non-clathrin/caveolin mediated endocytosis as a mediator of amyloid regulation. Via knockdown models, they were able to show, with convincing image detail, that amyloid precursor protein (APP) internalization was reduced in the absence of flotillin-2. Furthermore, the increased resolution also permitted measurement of membrane-bound APP clusters with 70nm precision, and revealed that flotillin knockdown significantly reduced APP cluster size (Schneider, et al., 2008).

Additionally, Barrantes and colleagues successfully probed the nanoscale arrangement of acetylcholine receptors using STED microscopy (Kellner, et al., 2007). Perturbations in plasma membrane cholesterol via methyl- β -cyclodextrin resulted in significant, yet sub-diffraction changes in receptor behaviour, with clear implications for their regulation via endocytosis (Barrantes, 2007).

In combination with the development of video rate STED microscopy (Westphal, et al., 2008), Hell and colleagues were able to dynamically image synaptic vesicle trafficking in neurons at 40-60nm resolution (Willig, Rizzoli, et al., 2006). While synaptic transmission is often treated as an exocytic phenomenon, these results indicated that synaptotagmin remains clustered after exocytic vesicle fusion with the neuronal plasma membrane. This observation has clear implications for neurotransmitter re-endocytosis, as the precise mechanism by which endosomal recycling controls neurotransmitter release is still under investigation. These results indicate that membrane re-sorting of neurotransmitters may not

be necessary for their recycling back to the cytoplasm. Via multi-temperature immunolabeling, combined with appropriate blocking and permeabilization, these data indicated re-endocytosis of synaptotagmin occurred within seconds of their initial exocytosis. Below, Figure 8 shows the increase in image quality afforded by STED when imaging re-endocytosed synaptic vesicles, taken from (Willig, Rizzoli, et al., 2006).

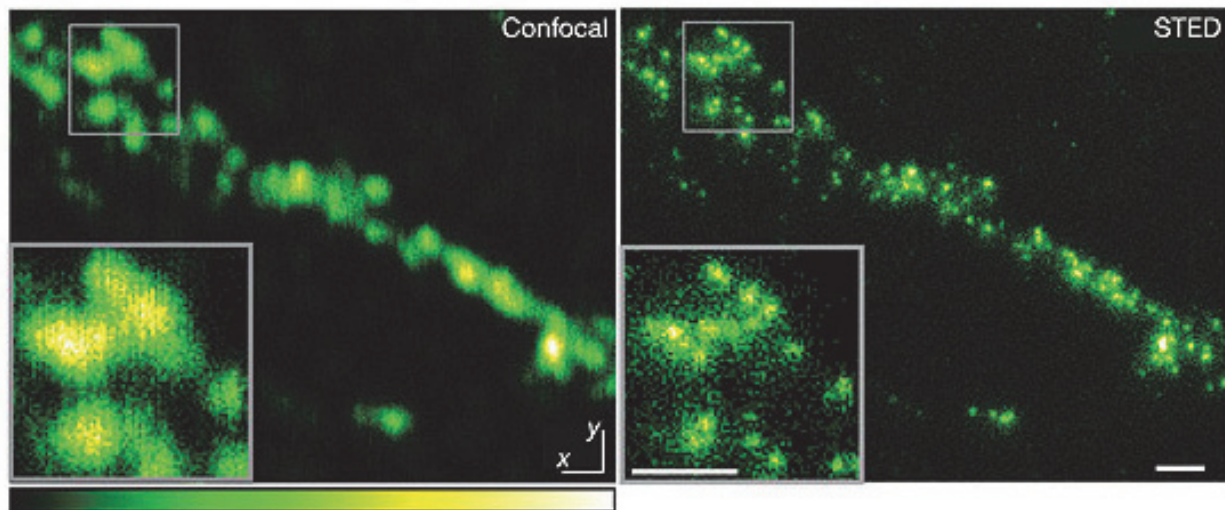


Figure 8. Confocal (left) and STED (right) microscopy images of synaptotagmin clustering on the surface of neuronal cells. STED microscopy affords a nearly order of magnitude increase in image resolution, allowing better quantification of neurotransmitter clustering, thereby giving better insight into the role of re-endocytosis as a mediator of synaptic transmission (Willig, Rizzoli, et al., 2006). Reprinted by permission from Macmillan Publishers Ltd: Nature K.I. Willig et al., **440**, 935-939, ©2006

4. Spectral imaging

4.1. Basic principles

Traditionally, optical microscopy (including the confocal and TIRF modalities applied to applications in endocytosis), and even superresolution imaging have been accomplished using a set of one or more filters to select a specific range of emission wavelengths to pass on to the detector. Filter-based microscopy is readily commercially available and can be extremely fast, producing high quality images at frame rates of up to hundreds or thousands of Hz with modern detectors. Filter-based microscopy requires that multiple chromophores of interest have well-separated emissions in order to avoid a phenomenon known as spectral channel crosstalk or spectral bleed through (SBT). Thoughtful choices of fluorophore labels can permit two- or three-color imaging in well characterized systems with filter-based microscopes; however in most live cell applications, filter-based microscopy is further limited by the presence of cellular autofluorescence. Cellular autofluorescence typically displays a broad emission that can span most of the visible wavelengths, and its spectral characteristics and intensity can vary widely across cell types and even within cells. In many applications where sensitivity is not a limiting factor, thresholding is used to minimize the SBT effect of cellular autofluorescence. Unfortunately,

thresholding approaches may not be suitable for imaging of endocytotic processes if the signal at the single event level is often very near the intensity level of the cellular autofluorescence, since this will greatly confound quantitative analyses.

Spectral imaging is an alternative to filter-based microscopy whereby an entire emission spectrum is collected at each image pixel (2D) or voxel (3D) (Garini, et al., 2006; Zimmerman, et al., 2003). Spectral imaging has been implemented in a variety of optical modalities for biological applications including visible reflectance (Zuzak, et al., 2002), fluorescence (Michalet, et al., 2003) and vibrational spectroscopies such IR absorption (Levin & Bhargava, 2005), Raman scattering (Christensen & Morris, 1998), and surface-enhanced Raman (SERS) (Sharonov, et al., 1994)), as well as in non-optical methods like mass spectrometry (Fletcher, et al., 2008). In practice, higher degrees of multiplexing, higher accuracy, and lower detection limits are achievable with spectral imaging due to the ability to implement multivariate analysis methods to identify and/or classify spectral signatures even in the presence of high degrees of spectral overlap from other labels and cellular autofluorescence (Mansfield, et al., 2005). The trade-off is usually a sacrifice in speed, however microscope designs have been recently introduced that are competitive with current filter-based microscope acquisition rates (Sinclair, et al., 2006). In addition, further advances in the speed of acquisition are possible and anticipated given the latest detector technology (Coates, 2011; Fowler, et al., 2010).

Of the spectral imaging modalities, fluorescence and Raman-based spectral imaging are of particular interest to the field of endocytosis due to their demonstrated success in increasing the degree of multiplexing and providing label-free molecular specificity, respectively. Lerner provides a comprehensive tutorial covering the general principles of imaging spectrometers applicable to both fluorescence and Raman modalities and the reader is referred there for additional information (Lerner, 2006).

Fluorescence spectral imaging, also termed hyperspectral fluorescence microscopy, can be implemented in a wide variety of formats that differ predominantly in the way the spectral information is obtained. Hyperspectral fluorescence microscopes typically use one of three approaches to generate spectrally-resolved information: (1) a prism or grating to disperse the fluorescence emission onto a linear detector array or a charge-coupled device (CCD) detector in point-scanning (Sinclair, et al., 2006) or line-scanning (Sinclair, et al., 2004) formats, (2) interferometric methods that measure the intensity as a function of optical path length difference and glean spectral information through Fourier analysis (Malik, et al., 1996), (3) sequential, narrow bandpass filter scanning of discrete wavelength regions using acousto-optical or liquid crystal tunable filter (Gat, 2000).

4.2. Applications of fluorescence spectral imaging in endocytosis

Due to their relatively large excitation cross section, size-determined emission properties, and improved photostability as compared with traditional organic fluorophores, semiconductor quantum dots (QDs) are becoming increasingly popular for biomedical research,

with applications including targeted therapeutics and disease diagnostics. However the behavior and ultimate fate of these and other engineered nanoparticles in living systems has yet to be fully characterized. To this end, Aaron and co-authors took advantage of the multiplexing capabilities of hyperspectral confocal fluorescence microscopy and multivariate curve resolution (MCR), a constrained alternating least squares method, to identify and localize three colors of quantum dots and a lysosome-specific dye simultaneously (Aaron, et al., 2011), as shown in Figure 9. This work revealed unanticipated compartmentalization of the QDs on the plasma membrane (B and D) of a non-phagocytotic immune cell line (RBL cells), as well as an accurate measure of the relative fraction of QDs located within the lysosomes following endocytosis (C). These data were acquired with high precision, despite the significant spectral overlap between the various QDs and the lysosome-specific tracer dye, as shown in (A).

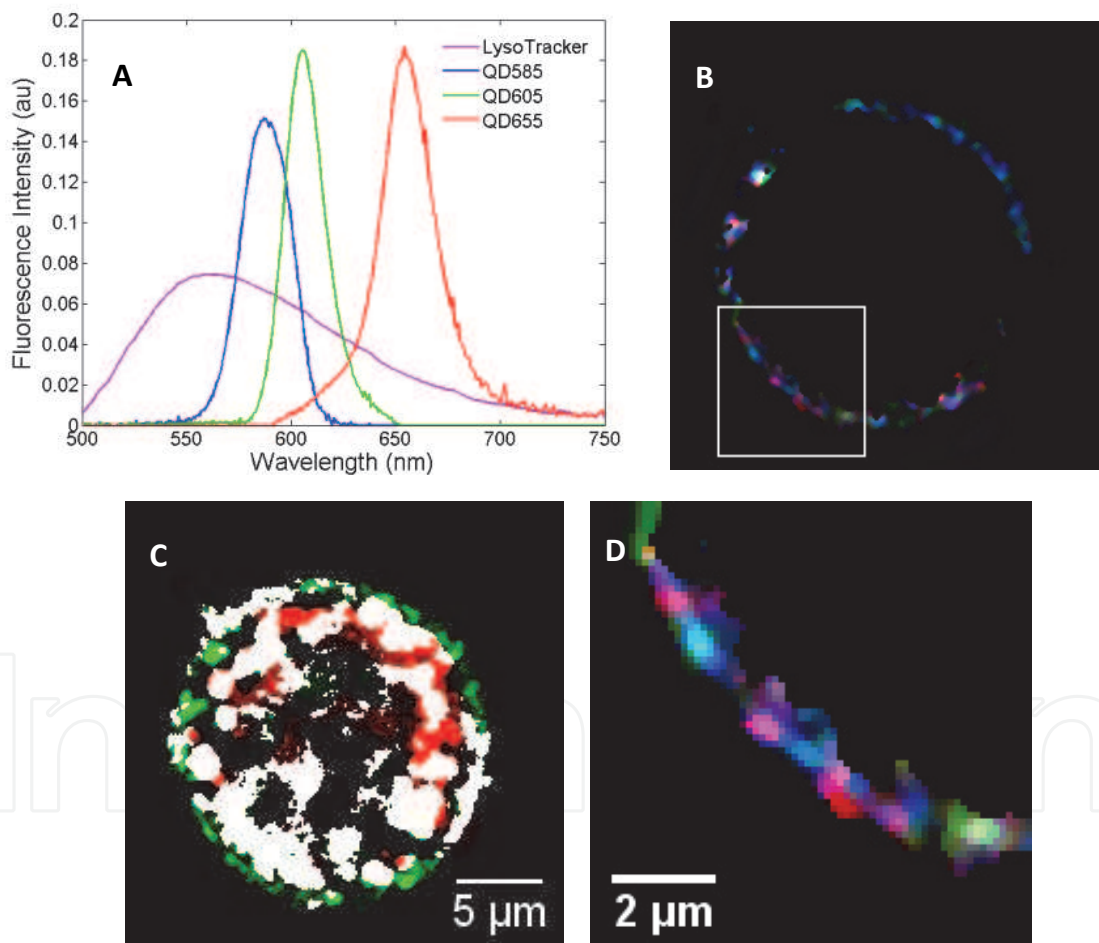


Figure 9. Hyperspectral imaging of quantum dot (QD) endocytosis. In (A), pure component spectra for three sized/shaped of QDs and a lysosome-specific fluorescent tracer are calculated without the need for any a priori information, and despite significant spectral overlap. (B) indicates QDs not present in lysosomes, with the white box denoting the enlarged region shown in (D). Images indicate a compartmentalization of similar sized/ shaped QDs into distinct regions near the membrane, rather than a random distribution. In (C), QD signal is shown in green, while lysosome-specific dye is indicated in red. Areas of QD/lysosome co-localization are shown in white.

Huth and colleagues have also demonstrated the power of fluorescence hyperspectral imaging for visualizing uptake and intracellular trafficking of liposomes (Huth, et al., 2004). This work has particular relevance to understanding and manipulating the mechanisms of drug delivery via liposomal vehicles. They utilized Fourier-transform based spectral imaging technology to generate hyperspectral images of five fluorescent dyes in COS-7 cells. With the help of multivariate analysis algorithms, they were able to determine vesicle distribution throughout the cell relative to membrane lipids, lysosomes, and nuclear compartments. Their work clearly shows the multiplexing and accuracy advantages of spectral imaging for visualizing multiple subcellular compartments, while following the distribution of endocytosed cargo.

These highlighted applications illustrate the suitability of hyperspectral fluorescence microscopy for fundamental research into endocytotic mechanisms and make it easy to imagine future work employing hyperspectral fluorescence microscopy to follow the distributions of many of the cellular factors listed in Table 1 of Mercer (Mercer, et al., 2010), as well as potential cargo with diffraction-limited spatial and moderate temporal (10-100's of frame/sec) resolution. Studies of this type would provide information unavailable with other techniques.

4.3. Applications of Raman spectral imaging in endocytosis

Unlike fluorescence spectral imaging, Raman spectral imaging does not typically utilize exogenous labels to generate image contrast (Lewis & Edwards, 2001). Instead, the technique relies on the interaction of excitation light with the native molecular vibrations that are characteristic of distinct molecular components within the sample. These molecular "signatures" provide a label-free detection method for many important biomolecules, including proteins, nucleic acids, lipids, phospholipids, and carbohydrates. Though Raman spectral signatures are much weaker than fluorescence emission spectra, it is possible to perform Raman spectral imaging at the single cell level with modern detection technologies. Hyperspectral Raman microscopy can be implemented in a variety of formats similar to those described for hyperspectral fluorescence microscopy (Christensen & Morris, 1998; Govil, et al., 1993; Morris, et al., 1996), however the most commonly utilized for visualizing endocytosis in living cells has been the confocal point-scanning method, due to its availability, high sensitivity, optical sectioning capability, and speed.

Chernenko and colleagues applied hyperspectral confocal Raman microscopy to noninvasively query the distribution of cellular organelles relative to two biodegradable polymeric nanoparticle delivery systems (Chernenko, et al., 2009). It is very important to characterize the biocompatibility, cellular uptake and intracellular trafficking of these and other nanoparticle vehicles for drug delivery. Typically this is accomplished through the use of 1-2 fluorescent labels at a time and as such is likely to be inefficient and can suffer problems with label stability and interference with the nanocarrier. Importantly, in addition

to the multiplexed advantage demonstrated with fluorescence-based spectral imaging, Raman spectra are exquisitely sensitive to changes in the local biochemical environment. This gives the added ability to detect and monitor changes that are associated with nanoparticle degradation (such as endosomal acidification). The authors employed a multivariate analysis algorithm known as Vertex Component Analysis to decompose spectra into their individual components (also called endmembers) (Nascimento & Dias, 2005). The resulting data were able to represent the spatial distribution of proteins, nanoparticles, lipid/phospholipids rich organelle membranes, and endosomal vesicles all without the need for exogenous labels.

Toward similar goals of characterizing the endocytotic uptake and trafficking of gold nanoparticles for applications in biomedical diagnostics and targeted gene/drug delivery, Park et al. used surface-enhanced Raman scattering (SERS) and dark field microscopy to visualize gold nanoparticles conjugated to transferrin protein (Park, et al., 2011). This work demonstrates the additional sensitivity offered by SERS over traditional Raman spectroscopy, and the potential of this method to not only follow nanoparticle distribution in three dimensions in a single living cell, but also make use of SERS spectral changes to indicate alterations in protein conjugation due to biochemical reactions.

5. Conclusion

A fuller understanding of endocytosis processes and the signalling cascades that regulate them is critically important for developing diagnostics, therapeutics, and vaccines. In this chapter we have presented three advanced optical imaging methodologies that have demonstrated advantages in spatial, temporal, and/or spectral resolution over traditional microscopy for interrogation of the processes involved in cellular uptake and trafficking. The ability to visualize dynamics of multiple species within living cells with high 3D spatial and temporal resolution provides unique information about molecular level interactions and their heterogeneity, both within and between cells, that is unavailable with other techniques. The examples we highlighted from recent literature illustrate how these tools are being engaged to address unanswered questions about the roles of key biomolecules including actin, dynamin, and others in the field of endocytosis as well as the sequence of biomolecular events during cellular response.

Yet, the potential of advanced imaging for studying endocytosis-related processes has not been fully realized. Recent developments in super-resolution microscopy, spectral imaging, and specialized TIRF modalities have extended imaging into a realm where multiple biomolecules involved in individual endocytic events can be visualized with never before seen clarity, detail, and precision. Future efforts will doubtlessly focus on continued improvements to these enabling technologies individually, as well as on coupling the aforementioned approaches. Progress towards both ends will provide more complete visualizations that are necessary to complement bulk biochemical and genetic approaches, and thus better characterize endocytosis pathways in the living cell.

Author details

Jesse S. Aaron and Jerilyn A. Timlin
Sandia National Laboratories, USA

Acknowledgement

Sandia National Laboratories is a multi-program laboratory managed and operated by Sandia Corporation, a wholly owned subsidiary of Lockheed Martin Corporation, for the U.S. Department of Energy's National Nuclear Security Administration under contract DE-AC04-94AL85000. This work was supported by the National Institutes of Health Director's New Innovator Award Program, 1-DP2-OD006673-01 (JSA and JAT). We would also like to acknowledge Ms. Michelle Raymer for helpful assistance in preparing this manuscript.

6. References

- Aaron, J.S., Greene, A.C., Kotula, P.G., Bachand, G.D., & Timlin, J.A. (2011). Advanced Optical Imaging Reveals the Dependence of Particle Geometry on Interactions Between CdSe Quantum Dots and Immune Cells. *Small*, Vol.7, No.3, pp. 334-341. 1613-6829
- Abbe, E. (1873). Beiträge zur Theorie des Mikroskops und der mikroskopischen Wahrnehmung. *Archiv für Mikroskopische Anatomie*, Vol.9, No.1, pp. 413-418. 0176-7364
- Anantharam, A., Onoa, B., Edwards, R.H., Holz, R.W., & Axelrod, D. (2010). Localized topological changes of the plasma membrane upon exocytosis visualized by polarized TIRFM. *The Journal of Cell Biology*, Vol.188, No.3, February 8, 2010, pp. 415-428.
- Axelrod, D. (1981). Cell-substrate contacts illuminated by total internal reflection fluorescence. *The Journal of Cell Biology*, Vol.89, No.1, April 1, 1981, pp. 141-145.
- Axelrod, D. (2001). Total Internal Reflection Fluorescence Microscopy in Cell Biology. *Traffic*, Vol.2, No.11, pp. 764-774. 1600-0854
- Barrantes, F.J. (2007). Cholesterol effects on nicotinic acetylcholine receptor. *Journal of Neurochemistry*, Vol.103, No.pp. 72-80. 1471-4159
- Betz, W.J., Mao, F., & Smith, C.B. (1996). Imaging exocytosis and endocytosis. *Current Opinion in Neurobiology*, Vol.6, No.3, pp. 365-371. 0959-4388
- Betzig, E., Patterson, G.H., Sougrat, R., Lindwasser, O.W., Olenych, S., Bonifacino, J.S., et al. (2006). Imaging intracellular fluorescent proteins at nanometer resolution. *Science*, Vol.313, No.5793, Sep, pp. 1642-1645.
- Boehm, M., & Bonifacino, J.S. (2001). Adaptins. *Molecular Biology of the Cell*, Vol.12, No.10, October 1, 2001, pp. 2907-2920.
- Brandenburg, B., Lee, L.Y., Lakadamyali, M., Rust, M.J., Zhuang, X., & Hogle, J.M. (2007). Imaging Poliovirus Entry in Live Cells. *PLoS Biology*, Vol.5, No.7, pp. e183.
- Brandenburg, B., & Zhuang, X. (2007). Virus trafficking - learning from single-virus tracking. [10.1038/nrmicro1615]. *Nature Reviews Microbiology*, Vol.5, No.3, pp. 197-208. 1740-1526
- Chan, W.C.W., & Nie, S. (1998). Quantum Dot Bioconjugates for Ultrasensitive Nonisotopic Detection. *Science*, Vol.281, No.5385, September 25, 1998, pp. 2016-2018.

- Chernenko, T., Matthäus, C., Milane, L., Quintero, L., Amiji, M., & Diem, M. (2009). Label-Free Raman Spectral Imaging of Intracellular Delivery and Degradation of Polymeric Nanoparticle Systems. *ACS Nano*, Vol.3, No.11, 2009/11/24, pp. 3552-3559. 1936-0851
- Christensen, K.A., & Morris, M.D. (1998). Hyperspectral Raman microscopic imaging using Powell lens line illumination. *Applied Spectroscopy*, Vol.52, No.9, 1998, pp. 1145-1147.
- Coates, C. (2011). New sCMOS vs. Current Microscopy Cameras: Andor Technology.
- Dempsey, G.T., Vaughan, J.C., Chen, K.H., Bates, M., & Zhuang, X. (2011). Evaluation of fluorophores for optimal performance in localization-based super-resolution imaging. [10.1038/nmeth.1768]. *Nature Methods*, Vol.8, No.12, pp. 1027-1036. 1548-7091
- Ehrlich, M., Boll, W., van Oijen, A., Hariharan, R., Chandran, K., Nibert, M.L., et al. (2004). Endocytosis by Random Initiation and Stabilization of Clathrin-Coated Pits. *Cell*, Vol.118, No.5, pp. 591-605. 0092-8674
- Fletcher, J.S., Rabbani, S., Henderson, A., Blenkinsopp, P., Thompson, S.P., Lockyer, N.P., et al. (2008). A New Dynamic in Mass Spectral Imaging of Single Biological Cells. *Analytical Chemistry*, Vol.80, No.23, pp. 9058-9064.
- Floyd, D.L., Ragains, J.R., Skehel, J.J., Harrison, S.C., & van Oijen, A.M. (2008). Single-particle kinetics of influenza virus membrane fusion. *Proceedings of the National Academy of Sciences*, Vol.105, No.40, October 7, 2008, pp. 15382-15387.
- Fowler, B., Liu, C., Mims, S., Balicki, J., Li, W., Do, H., et al. (2010). A 5.5Mpixel 100 frames/sec wide dynamic range low noise CMOS image sensor for scientific applications. *Proceedings of SPIE*, 9780819479297, San Jose, CA, Jan 2010.
- Gaidarov, I., Santini, F., Warren, R.A., & Keen, J.H. (1999). Spatial control of coated-pit dynamics in living cells. [10.1038/8971]. *Nature Cell Biology*, Vol.1, No.1, pp. 1-7. 1465-7392
- Gao, X., Yang, L., Petros, J.A., Marshall, F.F., Simons, J.W., & Nie, S. (2005). In vivo molecular and cellular imaging with quantum dots. *Current Opinion in Biotechnology*, Vol.16, No.1, pp. 63-72. 0958-1669
- Garini, Y., Young, I.T., & McNamara, G. (2006). Spectral imaging: Principles and applications. *Cytometry Part A*, Vol.69A, No.8, pp. 735-747. 1552-4930
- Gat, N. (2000). Imaging Spectroscopy Using Tunable Filters: A Review. *Proceedings of Wavelet Applications VII*.
- Govil, A., Pallister, D.M., & Morris, M.D. (1993). Three-dimensional confocal Raman microscopy. *Applied Spectroscopy*, Vol.47, No.1, 1993, pp. 75-79.
- Hashida, M., Kawakami, S., & Yamashita, F. (2005). Lipid Carrier Systems for Targeted Drug and Gene Delivery. *Chemical and Pharmaceutical Bulletin*, Vol.53, No.8, pp. 871-880.
- He, Y., Li, H.-W., & Yeung, E.S. (2005). Motion of Single DNA Molecules at a Liquid-Solid Interface As Revealed by Variable-Angle Evanescent-Field Microscopy. *The Journal of Physical Chemistry B*, Vol.109, No.18, 2005/05/01, pp. 8820-8832. 1520-6106
- Hell, S.W., & Wichmann, J. (1994). Breaking the diffraction resolution limit by stimulated emission: stimulated-emission-depletion fluorescence microscopy. *Optics Letters*, Vol.19, No.11, pp. 780-782.

- Hess, S.T., Girirajan, T.P.K., & Mason, M.D. (2006). Ultra-High Resolution Imaging by Fluorescence Photoactivation Localization Microscopy. *Biophysical Journal*, Vol.91, No.11, December 1, 2006, pp. 4258-4272.
- Hoekstra, D., De Boer, T., Klappe, K., & Wilschut, J. (1984). Fluorescence method for measuring the kinetics of fusion between biological membranes. *Biochemistry*, Vol.23, No.24, 1984/11/01, pp. 5675-5681. 0006-2960
- Huang, B., Bates, M., & Zhuang, X. (2009). Super-resolution fluorescence microscopy. *Annual Review of Biochemistry*, Vol.78, No.pp. 993-1016. 1545-4509 (Electronic)
- Huang, B., Jones, S.A., Brandenburg, B., & Zhuang, X. (2008). Whole-cell 3D STORM reveals interactions between cellular structures with nanometer-scale resolution. [10.1038/nmeth.1274]. *Nature Methods*, Vol.5, No.12, pp. 1047-1052. 1548-7091
- Huang, B., Wang, W., Bates, M., & Zhuang, X. (2008). Three-Dimensional Super-Resolution Imaging by Stochastic Optical Reconstruction Microscopy. *Science*, Vol.319, No.5864, February 8, 2008, pp. 810-813.
- Huth, U., Wieschollek, A., Garini, Y., Schubert, R., & Peschka-Süss, R. (2004). Fourier transformed spectral bio-imaging for studying the intracellular fate of liposomes. *Cytometry Part A*, Vol.57A, No.1, pp. 10-21. 1552-4930
- Johannsdottir, H.K., Mancini, R., Kartenbeck, J., Amato, L., & Helenius, A. (2009). Host Cell Factors and Functions Involved in Vesicular Stomatitis Virus Entry. *Journal of Virology*, Vol.83, No.1, January 1, 2009, pp. 440-453.
- Juette, M.F., Gould, T.J., Lessard, M.D., Mlodzianoski, M.J., Nagpure, B.S., Bennett, B.T., et al. (2008). Three-dimensional sub-100 nm resolution fluorescence microscopy of thick samples. [10.1038/nmeth.1211]. *Nature Methods*, Vol.5, No.6, pp. 527-529. 1548-7091
- Kaksonen, M., Toret, C.P., & Drubin, D.G. (2006). Harnessing actin dynamics for clathrin-mediated endocytosis. [10.1038/nrm1940]. *Nature Reviews Molecular Cell Biology*, Vol.7, No.6, pp. 404-414. 1471-0072
- Kellner, R.R., Baier, C.J., Willig, K.I., Hell, S.W., & Barrantes, F.J. (2007). Nanoscale organization of nicotinic acetylcholine receptors revealed by stimulated emission depletion microscopy. *Neuroscience*, Vol.144, No.1, pp. 135-143. 0306-4522
- Keyel, P.A., Watkins, S.C., & Traub, L.M. (2004). Endocytic Adaptor Molecules Reveal an Endosomal Population of Clathrin by Total Internal Reflection Fluorescence Microscopy. *Journal of Biological Chemistry*, Vol.279, No.13, March 26, 2004, pp. 13190-13204.
- Kiessling, V., Domanska, M.K., & Tamm, L.K. (2010). Single SNARE-Mediated Vesicle Fusion Observed In Vitro by Polarized TIRFM. *Biophysical Journal*, Vol.99, No.12, pp. 4047-4055. 0006-3495
- Kirchhausen, T., Harrison, S.C., & Heuser, J. (1986). Configuration of clathrin trimers: Evidence from electron microscopy. *Journal of Ultrastructure and Molecular Structure Research*, Vol.94, No.3, pp. 199-208. 0889-1605
- Klar, T.A., Jakobs, S., Dyba, M., Egner, A., & Hell, S.W. (2000). Fluorescence microscopy with diffraction resolution barrier broken by stimulated emission. *Proceedings of the National Academy of Sciences*, Vol.97, No.15, July 18, 2000, pp. 8206-8210.

- Lakadamyali, M., Rust, M.J., Babcock, H.P., & Zhuang, X. (2003). Visualizing infection of individual influenza viruses. *Proceedings of the National Academy of Sciences*, Vol.100, No.16, August 5, 2003, pp. 9280-9285.
- Lehmann, M., Rocha, S., Mangeat, B., Blanchet, F., Uji-i, H., Hofkens, J., et al. (2011). Quantitative Multicolor Super-Resolution Microscopy Reveals Tetherin HIV-1 Interaction. *PLoS Pathog*, Vol.7, No.12, pp. e1002456.
- Lerner, J.M. (2006). Imaging spectrometer fundamentals for researchers in the biosciences— A tutorial. *Cytometry Part A*, Vol.69A, No.8, pp. 712-734. 1552-4930
- Leserman, L.D., Weinstein, J.N., Blumenthal, R., & Terry, W.D. (1980). Receptor-mediated endocytosis of antibody-opsonized liposomes by tumor cells. *Proceedings of the National Academy of Sciences*, Vol.77, No.7, July 1, 1980, pp. 4089-4093.
- Levin, I.W., & Bhargava, R. (2005). Fourier Transform Infrared Vibrational Spectroscopic Imaging: Integrating Microscopy and Molecular Recognition. *Annual Review of Physical Chemistry*, Vol.56, No.1, pp. 429-474.
- Lewis, I.R., & Edwards, H.G.M. (2001). Handbook of Raman Spectroscopy *Practical Spectroscopy Series* (pp. 1074). New York: Marcel Dekker, Inc.
- Malik, Z., Cabib, D., Buckwald, R.A., Talmi, A., Garini, Y., & Lipson, S.G. (1996). Fourier transform multipixel spectroscopy for quantitative cytology. *Journal of Microscopy*, Vol.182, No.2, pp. 133-140. 1365-2818
- Manley, S., Gillette, J.M., Patterson, G.H., Shroff, H., Hess, H.F., Betzig, E., et al. (2008). High-density mapping of single-molecule trajectories with photoactivated localization microscopy. [10.1038/nmeth.1176]. *Nature Methods*, Vol.5, No.2, pp. 155-157. 1548-7091
- Mansfield, J.R., Gossage, K.W., Hoyt, C.C., & Levenson, R.M. (2005). Autofluorescence removal, multiplexing, and automated analysis methods for in-vivo fluorescence imaging. *Journal of Biomedical Optics*, Vol.10, No.4, pp.
- Marquis, B.J., Love, S.A., Braun, K.L., & Haynes, C.L. (2009). Analytical methods to assess nanoparticle toxicity. *Analyst*, Vol.134, No.3, pp. 425-439. 0003-2654
- Mattheyses, A.L., & Axelrod, D. (2006). Direct measurement of the evanescent field profile produced by objective-based total internal reflection fluorescence. *Journal of Biomedical Optics*, Vol.11, No.1, pp. 014006-014007.
- Medintz, I.L., Uyeda, H.T., Goldman, E.R., & Mattoussi, H. (2005). Quantum dot bioconjugates for imaging, labelling and sensing. [10.1038/nmat1390]. *Nature Materials*, Vol.4, No.6, pp. 435-446. 1476-1122
- Mercer, J., Schelhaas, M., & Helenius, A. (2010). Virus Entry by Endocytosis. *Annual Reviews of Biochemistry*, Vol.79, No.pp. 803-833.
- Merrifield, C.J., Feldman, M.E., Wan, L., & Almers, W. (2002). Imaging actin and dynamin recruitment during invagination of single clathrin-coated pits. [10.1038/ncb837]. *Nature Cell Biology*, Vol.4, No.9, pp. 691-698. 1465-7392
- Merrifield, C.J., Perrais, D., & Zenisek, D. (2005). Coupling between Clathrin-Coated-Pit Invagination, Cortactin Recruitment, and Membrane Scission Observed in Live Cells. *Cell*, Vol.121, No.4, pp. 593-606. 0092-8674

- Michalet, X., Kapanidis, A.N., Laurence, T., Pinaud, F., Doose, S., Pfughoefft, M., et al. (2003). The power and prospects of fluorescence microscopies and spectroscopies. *Annual Review of Biophysics and Biomeolecular Structure*, Vol.32, No.pp. 161-182.
- Morris, H.R., Hoyt, C.C., Miller, P., & Treado, P.J. (1996). Liquid Crystal Tunable Filter Raman Chemical Imaging. *Applied Spectroscopy*, Vol.50, No.6, pp. 805-811.
- Muller, M. (2006). *Introduction to Confocal Microscopy* (second ed. Vol. TT69).SPIE Press, Bellingham, Washington.
- Nägerl, U.V., Willig, K.I., Hein, B., Hell, S.W., & Bonhoeffer, T. (2008). Live-cell imaging of dendritic spines by STED microscopy. *Proceedings of the National Academy of Sciences*, Vol.105, No.48, December 2, 2008, pp. 18982-18987.
- Nascimento, J.M.P., & Dias, J.M.B. (2005). Vertex Component Analysis: A Fast Algorithm to Unmix Hypersepctral Data. *IEEE Transactions on Geoscience and Remote Sensing*, Vol.43, No.4, pp. 898-910.
- Oheim, M., Loerke, D., Stühmer, W., & Chow, R.H. (1998). The last few milliseconds in the life of a secretory granule. *European Biophysics Journal*, Vol.27, No.2, pp. 83-98. 0175-7571
- Olveczky, B.P., Periasamy, N., & Verkman, A.S. (1997). Mapping fluorophore distributions in three dimensions by quantitative multiple angle-total internal reflection fluorescence microscopy. *Biophysical Journal*, Vol.73, No.5, pp. 2836-2847. 0006-3495
- Oreopoulos, J., & Yip, C.M. (2009). Probing Membrane Order and Topography in Supported Lipid Bilayers by Combined Polarized Total Internal Reflection Fluorescence-Atomic Force Microscopy. *Biophysical Journal*, Vol.96, No.5, pp. 1970-1984. 0006-3495
- Panyam, J., & Labhasetwar, V. (2003). Biodegradable nanoparticles for drug and gene delivery to cells and tissue. *Advanced Drug Delivery Reviews*, Vol.55, No.3, pp. 329-347. 0169-409X
- Park, J.-H., Park, J., Dembereldorj, U., Cho, K., Lee, K., Yang, S., et al. (2011). Raman detection of localized transferrin-coated gold nanoparticles inside a single cell. *Analytical and Bioanalytical Chemistry*, Vol.401, No.5, pp. 1635-1643. 1618-2642
- Rappoport, J.Z. (2008). Focusing on clathrin-mediated endocytosis. *Biochemical Journal*, Vol.412, No.pp. 415-523.
- Rappoport, J.Z., Benmerah, A., & Simon, S.M. (2005). Analysis of the AP-2 Adaptor Complex and Cargo During Clathrin-Mediated Endocytosis. *Traffic*, Vol.6, No.7, pp. 539-547. 1600-0854
- Rappoport, J.Z., Kemal, S., Benmerah, A., & Simon, S.M. (2006). Dynamics of clathrin and adaptor proteins during endocytosis. *American Journal of Physiology - Cell Physiology*, Vol.291, No.5, November 1, 2006, pp. C1072-C1081.
- Rappoport, J.Z., Simon, S., & Benmerah, A. (2004). Review Understanding Living Clathrin-Coated Pits. [Article]. *Traffic*, Vol.5, No.5, pp. 327-337. 13989219
- Rappoport, J.Z., Taha, B.W., Lemeer, S., Benmerah, A., & Simon, S.M. (2003). The AP-2 Complex Is Excluded from the Dynamic Population of Plasma Membrane-associated Clathrin. *Journal of Biological Chemistry*, Vol.278, No.48, November 28, 2003, pp. 47357-47360.

- Rappoport, J.Z., Taha, B.W., & Simon, S.M. (2003). Movement of Plasma-Membrane-Associated Clathrin Spots Along the Microtubule Cytoskeleton. *Traffic*, Vol.4, No.7, pp. 460-467. 1600-0854
- Reichert, W.M., Suci, P.A., Ives, J.T., & Andrade, J.D. (1987). Evanescent Detection of Adsorbed Protein Concentration-Distance Profiles: Fit of Simple Models to Variable-Angle Total Internal Reflection Fluorescence Data. *Applied Spectroscopy*, Vol.41, No.3, pp. 503-508.
- Rittweger, E., Han, K.Y., Irvine, S.E., Eggeling, C., & Hell, S.W. (2009). STED microscopy reveals crystal colour centres with nanometric resolution. [10.1038/nphoton.2009.2]. *Nature Photonics*, Vol.3, No.3, pp. 144-147. 1749-4885
- Rust, M.J., Bates, M., & Zhuang, X. (2006). Sub-diffraction-limit imaging by stochastic optical reconstruction microscopy (STORM). [10.1038/nmeth929]. *Nature Methods*, Vol.3, No.10, pp. 793-796. 1548-7091
- Rust, M.J., Lakadamyali, M., Zhang, F., & Zhuang, X. (2004). Assembly of endocytic machinery around individual influenza viruses during viral entry. [10.1038/nsmb769]. *Nature Structural Molecular Biology*, Vol.11, No.6, pp. 567-573. 1545-9993
- Schermelleh, L., Heintzmann, R., & Leonhardt, H. (2010). A guide to super-resolution fluorescence microscopy. *The Journal of Cell Biology*, Vol.190, No.2, July 26, 2010, pp. 165-175.
- Schmoranzner, J., Goulian, M., Axelrod, D., & Simon, S.M. (2000). Imaging Constitutive Exocytosis with Total Internal Reflection Fluorescence Microscopy. *The Journal of Cell Biology*, Vol.149, No.1, April 3, 2000, pp. 23-32.
- Schneider, A., Rajendran, L., Honsho, M., Gralle, M., Donnert, G., Wouters, F., et al. (2008). Flotillin-Dependent Clustering of the Amyloid Precursor Protein Regulates Its Endocytosis and Amyloidogenic Processing in Neurons. *The Journal of Neuroscience*, Vol.28, No.11, March 12, 2008, pp. 2874-2882.
- Sharonov, S., Nabiev, I., Chourpa, I., Feofanov, A., Valisa, P., & Manfait, M. (1994). Confocal three-dimensional scanning laser Raman-SERS-fluorescence microprobe. Spectral imaging and high-resolution applications. *Journal of Raman Spectroscopy*, Vol.25, No.7-8, pp. 699-707. 1097-4555
- Shroff, H., Galbraith, C.G., Galbraith, J.A., & Betzig, E. (2008). Live-cell photoactivated localization microscopy of nanoscale adhesion dynamics. [10.1038/nmeth.1202]. *Nature Methods*, Vol.5, No.5, pp. 417-423. 1548-7091
- Shtengel, G., Galbraith, J.A., Galbraith, C.G., Lippincott-Schwartz, J., Gillette, J.M., Manley, S., et al. (2009). Interferometric fluorescent super-resolution microscopy resolves 3D cellular ultrastructure. *Proceedings of the National Academy of Sciences*, Vol.106, No.9, March 3, 2009, pp. 3125-3130.
- Sieczkarski, S.B., & Whittaker, G.R. (2002a). Dissecting virus entry via endocytosis. *Journal of General Virology*, Vol.83, No.7, July 1, 2002, pp. 1535-1545.
- Sieczkarski, S.B., & Whittaker, G.R. (2002b). Influenza Virus Can Enter and Infect Cells in the Absence of Clathrin-Mediated Endocytosis. *Journal of Virology*, Vol.76, No.20, October 15, 2002, pp. 10455-10464.

- Sinclair, M.B., Haaland, D.M., Timlin, J.A., & Jones, H.D.T. (2006). Hyperspectral confocal microscope. *Applied Optics*, Vol.45, No.24, pp. 3283-3291.
- Sinclair, M.B., Timlin, J.A., Haaland, D.M., & Werner-Washburne, M. (2004). Design, construction, characterization, and application of a hyperspectral microarray scanner. *Applied Optics*, Vol.43, No.10, pp. 2079-2089.
- Slowing, I.I., Vivero-Escoto, J.L., Wu, C.-W., & Lin, V.S.Y. (2008). Mesoporous silica nanoparticles as controlled release drug delivery and gene transfection carriers. *Advanced Drug Delivery Reviews*, Vol.60, No.11, pp. 1278-1288. 0169-409X
- Stephens, D.J., & Allan, V.J. (2003). Light Microscopy Techniques for Live Cell Imaging. *Science*, Vol.300, No.5616, April 4, 2003, pp. 82-86.
- Stock, K., Sailer, R., Strauss, W.S.L., Lyttek, M., Steiner, R., & Schneckenburger, H. (2003). Variable-angle total internal reflection fluorescence microscopy (VA-TIRFM): realization and application of a compact illumination device. *Journal of Microscopy*, Vol.211, No.1, pp. 19-29. 1365-2818
- Subach, F.V., Patterson, G.H., Manley, S., Gillette, J.M., Lippincott-Schwartz, J., & Verkhusa, V.V. (2009). Photoactivatable mCherry for high-resolution two-color fluorescence microscopy. [10.1038/nmeth.1298]. *Nature Methods*, Vol.6, No.2, pp. 153-159. 1548-7091
- Sund, S.E., & Axelrod, D. (2000). Actin Dynamics at the Living Cell Submembrane Imaged by Total Internal Reflection Fluorescence Photobleaching. *Biophysical Journal*, Vol.79, No.3, pp. 1655-1669. 0006-3495
- Sund, S.E., Swanson, J.A., & Axelrod, D. (1999). Cell Membrane Orientation Visualized by Polarized Total Internal Reflection Fluorescence. *Biophysical Journal*, Vol.77, No.4, pp. 2266-2283. 0006-3495
- Testa, I., Wurm, C.A., Medda, R., Rothermel, E., von Middendorf, C., Fölling, J., et al. (2010). Multicolor Fluorescence Nanoscopy in Fixed and Living Cells by Exciting Conventional Fluorophores with a Single Wavelength. *Biophysical Journal*, Vol.99, No.8, pp. 2686-2694. 0006-3495
- Thompson, N.L., Drake, A.W., Chen, L., & Broek, W.V. (1997). Equilibrium, Kinetics, Diffusion and Self-Association of Proteins at Membrane Surfaces: Measurement by Total Internal Reflection Fluorescence Microscopy. *Photochemistry and Photobiology*, Vol.65, No.1, pp. 39-46. 1751-1097
- Thompson, N.L., McConnell, H.M., & Burhardt, T.P. (1984). Order in supported phospholipid monolayers detected by the dichroism of fluorescence excited with polarized evanescent illumination. *Biophysical Journal*, Vol.46, No.6, pp. 739-747. 0006-3495
- Thompson, R.E., Larson, D.R., & Webb, W.W. (2002). Precise Nanometer Localization Analysis for Individual Fluorescent Probes. *Biophysical Journal*, Vol.82, No.5, pp. 2775-2783. 0006-3495
- Tokunaga, M., Kitamura, K., Saito, K., Iwane, A.H., & Yanagida, T. (1997). Single Molecule Imaging of Fluorophores and Enzymatic Reactions Achieved by Objective-Type Total Internal Reflection Fluorescence Microscopy. *Biochemical and Biophysical Research Communications*, Vol.235, No.1, pp. 47-53. 0006-291X

- van der Schaar, H.M., Rust, M.J., Waarts, B.-L., van der Ende-Metselaar, H., Kuhn, R.J., Wilschut, J., et al. (2007). Characterization of the Early Events in Dengue Virus Cell Entry by Biochemical Assays and Single-Virus Tracking. *Journal of Virology*, Vol.81, No.21, November 1, 2007, pp. 12019-12028.
- West, J.L., & Halas, N.J. (2003). Engineered Nanomaterials for Biophotonics Applications: Improving Sensing, Imaging, and Therapeutics. *Annual Review of Biomedical Engineering*, Vol.5, No.1, pp. 285-292.
- Westphal, V., Rizzoli, S.O., Lauterbach, M.A., Kamin, D., Jahn, R., & Hell, S.W. (2008). Video-Rate Far-Field Optical Nanoscopy Dissects Synaptic Vesicle Movement. *Science*, Vol.320, No.5873, April 11, 2008, pp. 246-249.
- Wildanger, D., Rittweger, E., Kastrop, L., & Hell, S.W. (2008). STED microscopy with a supercontinuum laser source. *Opt. Express*, Vol.16, No.13, pp. 9614-9621.
- Willig, K.I., Harke, B., Medda, R., & Hell, S.W. (2007). STED microscopy with continuous wave beams. [10.1038/nmeth1108]. *Nature Methods*, Vol.4, No.11, pp. 915-918. 1548-7091
- Willig, K.I., Kellner, R.R., Medda, R., Hein, B., Jakobs, S., & Hell, S.W. (2006). Nanoscale resolution in GFP-based microscopy. [10.1038/nmeth922]. *Nature Methods*, Vol.3, No.9, pp. 721-723. 1548-7091
- Willig, K.I., Rizzoli, S.O., Westphal, V., Jahn, R., & Hell, S.W. (2006). STED microscopy reveals that synaptotagmin remains clustered after synaptic vesicle exocytosis. [10.1038/nature04592]. *Nature*, Vol.440, No.7086, pp. 935-939. 0028-0836
- Zimmerman, T., Rietdorf, J., & Pepperkok, R. (2003). Spectral imaging and its applications in live cell microscopy. [minireview]. *Federation of European Biochemical Societies Letters*, Vol.546, No.pp. 87-92.
- Zuzak, K.J., Schaeberle, M.D., Lewis, E.N., & Levin, I.W. (2002). Visible reflectance hyperspectral imaging: Characterization of a noninvasive, in vivo system for determining tissue perfusion. *Analytical Chemistry*, Vol.74, No.9, pp. 2021-2028.